Numerical modeling of complex femtosecond laser inscribed fiber gratings – comparison with experiment

C. Koutsides,[1,2], K. Kalli,[1,a], D. J. Webb[2], L. Zhang[2]

[1] Nanophotonics Research Laboratory, Cyprus University of Technology, 3036, Lemessos, Cyprus
[2] Photonics Research Group, Aston University, B4 7ET, Birmingham, United Kingdom

ABSTRACT

We present experimental studies and numerical modeling based on a combination of the Bidirectional Beam Propagation Method and Finite Element Modeling that completely describes the wavelength spectra of point by point femtosecond laser inscribed fiber Bragg gratings, showing excellent agreement with experiment. We have investigated the dependence of different spectral parameters such as insertion loss, all dominant cladding and ghost modes and their shape relative to the position of the fiber Bragg grating in the core of the fiber. Our model is validated by comparing model predictions with experimental data and allows for predictive modeling of the gratings. We expand our analysis to more complicated structures, where we introduce symmetry breaking; this highlights the importance of centered gratings and how maintaining symmetry contributes to the overall spectral quality of the inscribed Bragg gratings. Finally, the numerical modeling is applied to superstructure gratings and a comparison with experimental results reveals a capability for dealing with complex grating structures that can be designed with particular wavelength characteristics.

Keywords: Fiber optics and optical communications; fiber Bragg gratings, numerical modeling

1. INTRODUCTION

Fiber Bragg gratings (FBG) have been inscribed using femtosecond (fs) lasers with the phase mask or standard interferometric method [1] or point-by-point (PbP) [2]. The latter is the focus if this paper as it provides a useful means to produce flexible grating structures, with tailored grating length, pitch, and spectral response. The fs processing leads to refractive index changes that are confined to the laser beam focal volume, permitting the development of complex gratings, such as superimposed or sampled gratings [3]. This localized index change can be a drawback, as a small lateral shift of the focal point will displace the inscribed grating from fiber axis (off–axis inscription), changing the grating spectrum in strength and shape, because of symmetry breaking. It is important to predict how it will modify the FBG spectrum, and numerical modeling can become a strong tool to support the inscription process. To date there are no noteworthy studies of the grating spectra of fs laser inscribed gratings by the PbP method. We apply the bidirectional beam propagation method (BPM) and the finite element method (FEM), optimizing the solution convergence and accuracy for the propagating mode calculation. Our analysis predicts losses and gives prominence to the cladding mode spectra. We show that a lateral shift of the grating leads to an exponential reduction in FBG reflectivity, a concomitant modification of the cladding modes, and the growth of a ghost mode. The agreement between analysis and experimental results, allows us to accurately reproduce the physical grating parameters, such as the spatial extent and strength of the refractive index modulation, the grating length, its displacement from the core center and whether there is any device tilt.

2. SIMULATION METHOD

Bidirectional BPM is well suited to modelling coupled forward and backward waves, readily accounting for resonant effects of gratings [4]. The approach automatically includes the effects of guided and radiating fields, as well as mode coupling and conversion. We solve the Helmholtz equation under the scalar field assumption for monochromatic waves,

$$\frac{\partial^2\phi}{\partial x^2}+\frac{\partial^2\phi}{\partial y^2}+\frac{\partial^2\phi}{\partial z^2}+k(x,y,z)^2\phi=0 \qquad (1)$$

[a] kkalli@cytanet.com.cy

21st International Conference on Optical Fiber Sensors, edited by Wojtek J. Bock, Jacques Albert, Xiaoyi Bao,
Proc. of SPIE Vol. 7753, 77536Q · © 2011 SPIE · CCC code: 0277-786X/11/$18 · doi: 10.1117/12.885124

where k(x,y,z) = k_0 n(x,y,z) is the spatially dependent wavenumber, and the refractive index distribution is n(x,y,z). To determine the launch field we use the slowly varying envelope approximation (u is a slowly varying field proportional to the phase variation of Φ) and the scalar field Φ(x,y,z) can be calculated along the propagation direction,

$$\phi(x,y,z) = u(x,y,z)e^{i\bar{k}z} \tag{2}$$

To reduce the computation time and improve accuracy, we pre–calculate the supported mode using FEM, and the solution converges faster as the launch field is closer to the propagation mode. We note that FEM gives highly accurate solutions for the supported modes and the effective refractive index at each wavelength [5]. The guided wave propagation problem is divided into regions that are uniform along the propagation axis z, and the interfaces between these regions. At any point along the structure it is assumed that both forward and backward waves can exist, denoted by $u+$ (x, y, z) and $u-$ (x, y, z), respectively. In the uniform regions the forward and backward waves are decoupled, whilst the interfaces between these regions couple the forward and backward waves due to reflection. A transfer matrix approach is employed in which the individual matrices are differential operators, and we assume that both the forward and backward fields are known at the input; an overall transfer matrix, M, describes the system,

$$\begin{pmatrix} u^{+}_{out} \\ u^{-}_{out} \end{pmatrix} = M \begin{pmatrix} u^{+}_{in} \\ u^{-}_{in} \end{pmatrix} \tag{3}$$

The physical propagation problem requires two key pieces of information, the refractive index distribution, n(x,y,z), and the input wave field, u(x,y,z=0). Thereafter, the system dictates the wave field throughout the rest of the domain, u(x,y,z>0). Additional input is required in the form of numerical simulation parameters such as the finite computational domain, {x ∈ (xmin,xmax)}, {y ∈ (ymin,ymax)}, and {z ∈ (zmin,zmax)}, the transverse grid sizes, Δx; and Δy, the longitudinal step size, Δz. Clearly the calculation accuracy is determined by the computational spatial resolution, the error in the effective refractive index of the supported mode and the step in the wavelength domain.

3. SIMULATION AND EXPERIMENTAL RESULTS – A COMPARISON

For our experimental and computational analyses we focus on standard SMF–28. Fig. 1(a) shows the calculated dominant mode and its effective refractive index. This mode defines the launch field at the entrance to the fiber ($u+_{in}$) in the matrix problem (Eqn. 3). Fig. 1(b) shows a typical comparison between calculated and measured spectra in a fiber containing a Bragg grating. A first order grating was inscribed in the center of the core of a standard SMF-28 fiber, using a femtosecond laser system (HighQ Laser Femtoregen IC335) emitting 300 fs pulses at 1035 nm and operating at a repetition rate of 1 kHz. The light was focused with a Mitutoyo microscope objective (x50, NA 0.42). Key parameters of the grating such as the period and the size of the spots were measured using an optical microscope. The size of the core was set to be 8.3 μm and the grating period was 536 nm, whereas the spot width was 2 μm and the grating length 2 cm. As we can see from Fig. 1(b) the analysis predicts the exact number of the cladding modes with an average wavelength determination error of 0.05 nm, or 0.005 %. Furthermore, the small average deviation between calculated and measured insertion loss ($4.6\text{x}10^{-3}$dB) increases the reliability of the predictions. Small deviations of the analysis compared with the experiment relate to the differences of the spot shape associated with the index change. We assumed homogenous spots whereas the refractive index change has an inhomogeneous distribution, because of the nonlinear laser pulse-material interaction. For further investigation of the power of the analysis we have inscribed gratings with different characteristics, such as longer, non-centered gratings with different spot size. We observe in Fig. 2 that the main features of the transmission spectrum can be modeled even for non symmetric structures; of course there is a trade off between the complexity of the structure and the computation time.

Modeling structures with a low degree of symmetry is challenging and one may anticipate simulation results diverge from experimental data. We have simulated superimposed gratings in SMF-28, comparing them with experimental results. Fig. 3 (a) shows the analysis predicts 12 cladding modes between the gratings peaks, in good agreement with the experiment. The relative strength of the peaks, resonance wavelengths and spectral shape are in good agreement. The inset in Fig. 3 (a) shows an index profile of the superimposed gratings, with one located on the fiber's axis whereas there is a lateral shift of 3μm for the second. The grating periods are 0.532 μm and the spot size is 1 μm.

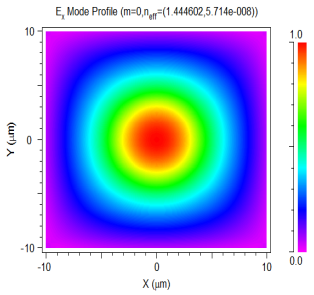

Fig 1. (a) Mode profile and fiber core refractive index

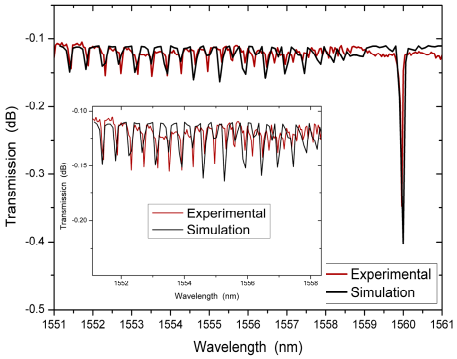

Fig. 1 (b) Typical experimental and simulated results

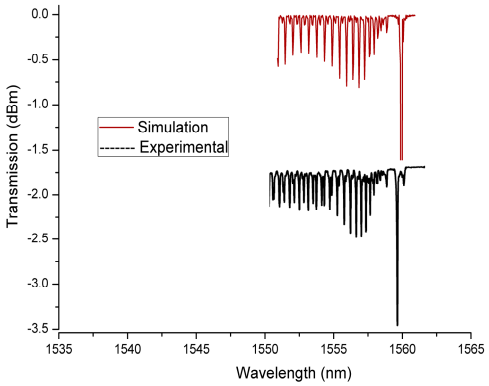

Fig. 2. Experimental and simulated results showing excellent agreement (traces offset for clarity)

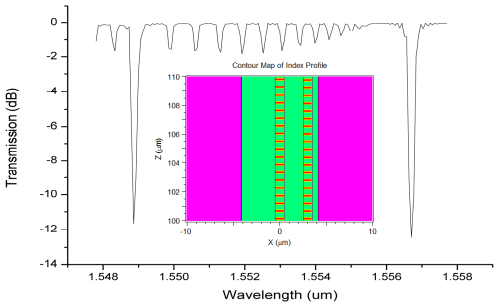

Fig. 3. (a) Simulated transmission spectrum of superimposed gratings (inset: FBG core positions)

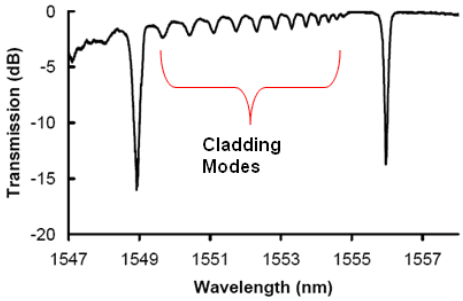

(b) Experimental spectrum

For Fig. 3, the FEM mesh is denser in order to extract sufficiently accurate solutions, and non–uniform meshing close to areas with small index contrast improves the solution accuracy. The accuracy algorithms heavily depend on the correct modeling of field variations that can be more pronounced near interfaces than in bulk regions. For complicated structures, computation cells on index interfaces were set to be five times smaller than for bulk regions. Finally, grid cells were set to be aligned in a symmetric way with respect to the interfaces between material regions.

Lateral shifts in the grating position break the structural symmetry and a strong “ghost mode” appears close to the grating wavelength, a spatial mode supported by the new geometry (Fig. 4). The reflectivity of the grating drops whilst the ghost mode increases proportionally and the asymmetry perturbs the lower order modes that are closer to the core. We also note that gratings inscribed at the core–cladding interface (boundary) display a stronger ghost mode with a simultaneous decay in Bragg reflectivity. Expanding our analysis we calculate the grating reflectivity according to the lateral shift from the center of the core, and observe for displacements greater than 1μm, the gradient of the slope increases rapidly leading to lower reflectivity even for small displacements; in agreement with experimental observations (Fig. 5). All previous analyses are based on the assumption that the grating is parallel to the fiber axis; in practice there is always some degree of grating tilt. As the angle increases the grating strength drops, ghost modes arise, and for small angles there is no spectral wavelength shift, Fig. 6. This symmetry distortion is less than when the entire grating was displaced. A very important observation is that there is an arbitrary change in cladding mode strength. At point A, cladding modes from less axially tilted gratings are stronger than those from parallel gratings, whereas at point B the opposite is true. This provides useful information on the grating position. Furthermore, phase mismatching appears even for very small rotations and that is translated to a drop in grating reflectivity. This fact reveals the importance of symmetry to the quality of the spectrum. Fig. 7 compares experimental measurements and modeling for a superstructure grating showing excellent agreement over the wavelength range; indicating that we have inscribed the superstructure very close to fiber’s axis.

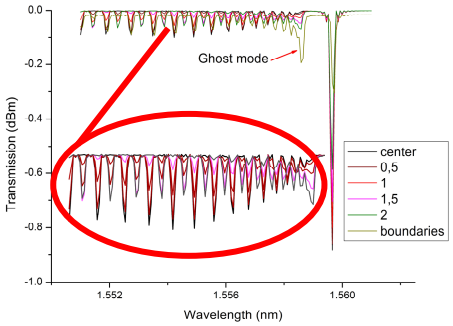

Fig. 4 Grating spectra for different grating offsets in microns (inset: cladding mode structure with greater clarity)

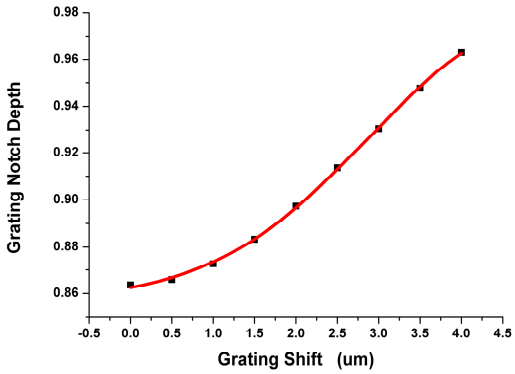

Fig. 5. Grating notch depth proportional to the position of the grating in the fiber core. Red line is a Gaussian fit to the data

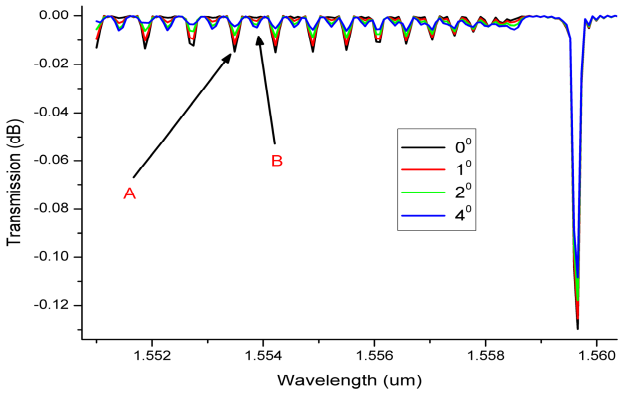

Fig. 6. Spectra for different grating angles (degree of axial tilt)

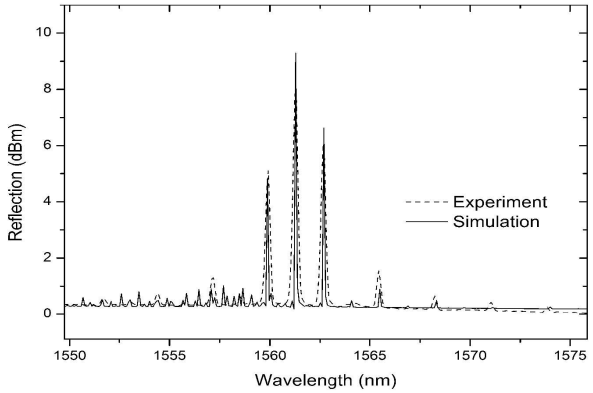

Fig. 7. SFBG experimental and theoretical transmission spectra

5. CONCLUSION

We have applied FEM and bidirectional BPM to completely describe the transmission spectra of PbP femtosecond laser inscribed FBGs, predicting all dominant spectral features that are strongly dependant on the FBG position in the core. Symmetry breaking is responsible for phase mismatching and the transmission spectrum can be affected even by a tiny rotation between the grating and fiber axes. Moreover, superstructure gratings have been successfully modeled. This analysis and approach can be used to improve and optimize the inscription of PbP fiber Bragg gratings that are simple or complex in nature. These results reveal the potential of the analysis and its use for PbP FBG inscription optimization.

ACKNOWLEDGEMENT

The authors acknowledge EU financial support via the project PHOSFOS (PHOtonic Skins For Optical Sensing).

REFERENCES

1 S. J. Mihailov, C. W. Smelser, P. Lu, R. B. Walker, D. Grobnic, H. Ding, G. Henderson and J. Unruh, "Fiber Bragg gratings made with a phase mask and 800-nm femtosecond radiation," Opt. Lett. **28**, 995-997 (2003)

2 A. Martinez, M. Dubov, I. Khrushchev and I. Bennion, "Direct writing of fibre Bragg gratings by femtosecond laser", Elec. Lett., **40**, 1170-1172 (2004)

3 A. Othonos and K. Kalli, *Fiber Bragg Gratings: fundamentals and applications in telecommunications and sensing* (Artech House Optoelectronics Library, 1999)

4 H. Rao, R. Scarmozzino and R. M. Osgood, "A bidirectional beam propagation method for multiple dielectric interfaces", IEEE Phot. Tech. Lett., 11, 830-832 (1999)

5 L. Vincetti, A. Cucinotta, S. Selleri and M. Zoboli "Three-dimensional finite-element beam propagation method: assessments and developments", J. Opt. Soc. Am. A, 17, 1124-1131 (2000)